Measurement of velocity induced by steam condensation into a water pool by tracking the motion of bubbles

Yun Feng, Xicheng Wang, Dmitry Grishchenko, and Pavel Kudinov
Division of Nuclear Engineering, Royal Institute of Technology, KTH
Corresponding Address
fengyun960106@gmail.com, xicheng@kth.se, dmitrygr@kth.se, pkudinov@kth.se

ABSTRACT

Pressure Suppression Pool (PSP) is employed in Boiling Water Reactor (BWR) as a heat sink to suppress pressurization of the containment and reactor vessel by discharging steam into the water pool. Modelling of Direct Contact Condensation (DCC) with the explicit resolution of both Mirco (condensation) and Macro (pool circulation) scales is computationally expensive, particularly for realistic plant analysis. Thus, Effective Heat Source (EHS) and Effective Momentum Source (EMS) models have been proposed to enable such prediction by using single-phase solver combined with empirical closures.

A Separate Effect Facility (SEF-POOL) has been designed to measure the time-averaged momentum (EMS). Latest analysis using large-scale pool data suggests that the velocity field induced by steam condensation plays an important role in setting boundary conditions and explaining the results of tests and simulations. Therefore, an experimental quantification approach for the measurement of velocity field induced by steam condensation is introduced. The measurement is achieved by stereo tracking of the air bubbles carried by the turbulent flow.

In this paper, we introduce the latest progress in the development of in-house code for bubble tracking and preliminary results of water to water and steam to water tests. CFD simulations are carried out to validate the measurement. The results suggest that the experimental approach can provide an adequate prediction of the axial velocity profiles. Turbulent flow induced by steam injection diffuses much faster than the single-phase turbulent flow with the same amount of momentum, indicating an extra turbulent kinetic energy source is necessary for setting the boundary conditions of EHS/EMS models.

KEYWORDS: ***Direct contact condensation, separate effect test, stereo bubble tracking, EHS/EMS models, CFD***

1. INTRODUCTION

Direct Contact Condensation (DCC) is applied to the light water reactor safety system to prevent pressurization of the reactor and containment. In Nordic BWR design [1], the steam can be released into a large water pool (Pressure Suppression Pool, PSP) through multi-hole sparger pipes that connect the reactor vessel and wetwell and blowdown pipes with a relatively larger diameter that connect drywell and wetwell (Figure 1). The performance of the safety system would be affected negatively if thermal stratification is developed in the pool during the operation. The development of thermal stratification is determined by the competition between the sources of momentum and heat. To enable the prediction of the pool behavior induced by DCC with affordable computational resources, Effective Heat/Momentum Sources (EHS/EMS) models have been proposed [2] and it has been successfully applied to the pool test simulations [3].

To measure the magnitude of effective momentum, a Separate Effect Facility (SEF-POOL) (Figure 4) was built and operated at Lappeenranta University of Technology (LUT), Finland. Several separate effect tests where steam is released through a single or multi-hole into a water pool have been performed to measure its induced momentum and investigate its relevant physical mechanisms [4]. More

specifically, the tests are used to determine the empirical correlation between the theoretical momentum rate of the injected steam and the effective momentum rate generated by the condensed water.

Direct measurement of velocity characteristics of steam condensation in a water phase is a challenging task, especially for the oscillatory bubble regime due to the rapid collapse of bubbles and significant temperature gradients. 2D Particle Image Velocimetry (PIV) with an $0.8 \times 0.8\ m^2$ Field of View (FOV) was used to measure the velocity field induced by the steam injection through a multi-hole sparger in PANDA facility [5-6]. The middle and far-field velocity are recorded (~300 mm away from the orifice) when the steam flow rate is $70\ kg/m^2s$. However, it becomes impossible to obtain the information of the main flow characteristics when the flow rate is increased to $115\ kg/m^2s$ or even higher. 3D PIV measurement was applied to HYMERES-2 PANDA H2P3 tests [7-8] but failed eventually. The particle density recorded by two cameras varies significantly and it might be caused by the high-temperature gradients that the light traveling from the particles experience different refractive indices during their passages toward two cameras.

The aim of the tests performed in the SEF-POOL is to provide database for the development and validation of the EMS model for the prediction of the time-averaged momentum induced by steam injection (both sub-sonic and sonic regimes) through single and multiple holes in PSP. EMS model introduces the single-phase effective liquid with the same momentum as steam condensation. Currently, the major uncertainty is the high-level turbulence [5] in the vicinity of the orifice that significantly diffuses the jet compared to the typical single-phase free shear flow with the same momentum. This uncertainty would affect the transfer of momentum and energy into the bulk pool and subsequently the development of thermal stratification or mixing in the pool [9-11].

The primary goal of this work is the development of the experimental approach for the measurement of velocity profiles induced by steam condensation jet to deduce the momentum transportation downstream of the flow. This measurement is enabled by injecting small air bubbles from the needles installed at the bottom of the pool and recoding its trajectories by stereo cameras. In-house code compiled by MATLAB [12] is used to segment, correlate and track bubbles to produce 3D trajectories and then uses these trajectories to estimate the flow velocity. The results are also compared with Computational Fluid Dynamics (CFD) simulations performed by ANSYS Fluent [13]. The tests discussed in this work are two types of tests (water to water and steam to water), aiming to verify the setup of the experiment (i.e., air generating system, stereo cameras) and image processing code.

The paper is organized as follows: Section 2 presents the theory of single-phase turbulent jet, Section 3 the configuration of facility and image processing, Section 4 the preliminary results and its comparison with CFD simulations, and Section 5 the conclusions.

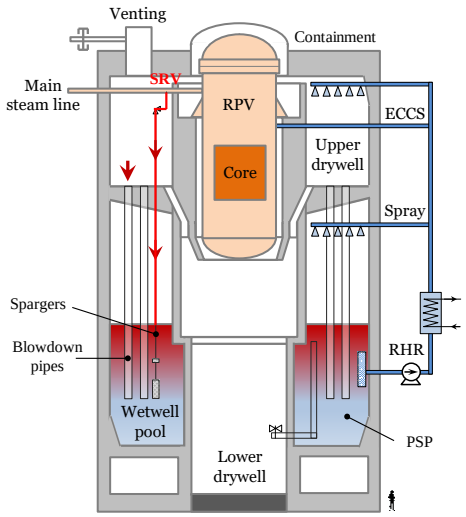

Figure 1 Nordic BWR containment [1]

2. SINGLE-PHASE TURBULENT JET AND EHS/EMS MODELS

Thermal behavior induced by the steam discharge through multi-hole spargers into a large pool was believed to be governed by the condensed jet [3]. The condensed liquid flow is the resultant jet produced by the steam condensed over a short distance. Given its similarity to the turbulent jet [14], an introduction of the single-phase turbulent jets is presented first and then follows a brief introduction of EHS/EMS models. Details information can be found in [10, 15].

2.1. Velocity Profiles of Single-Phase Turbulent

The jet being considered is a water jet discharged from a nozzle into a still tank filled with water. The schematic of the jet is shown in Figure 2. The axial velocity profile $U(x,r)$ can be expressed by Eq. (1) [16].

$$U(x,r) = \frac{U_0 B d}{(x-x_0)} e^{\left(-K\frac{r^2}{(x-x_0)^2}\right)} \tag{1}$$

where U_0 is the mean exit velocity, B the decay rate, d the nozzle diameter and x_0 the so-called virtual origin of the jet. The fully developed axisymmetric velocity profile obeys a law of self-similarity as described by Gaussian distribution. To integrate the square of velocity over the cross-section of the jet with the fluid density, the momentum rate of the jet is:

$$\dot{M} = \int_0^\infty \rho U(x,r)^2 2\pi r\, dr = \frac{1}{4}\pi d^2 \rho {U_0}^2 \cdot \frac{2B^2}{K} \tag{2}$$

Given the decay rate and expansion ratio are constant for a given jet and ignoring the energy dissipation, the jet momentum is conserved at any downstream cross-section of the jet and equal to its initial momentum $\pi d^2 \rho {U_0}^2/4$. Hence, we can deduce a rough relation between B and K as $2B^2 \sim$K, which shows that a jet with faster decay of the centerline velocity should also expand faster. Investigation of velocity characteristics induced by air, water, and steam jets shows for the fully developed jets $2B^2/K = 0.88 \sim 1.05$ [17].

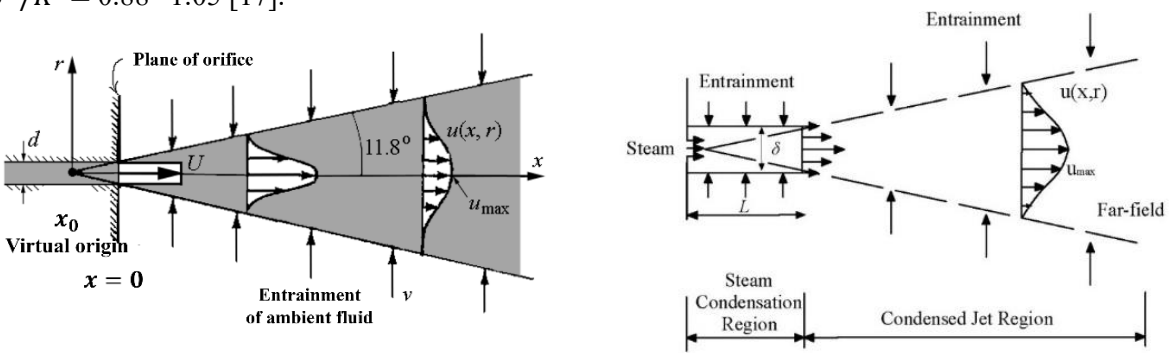

(a) **(b)**

Figure 2 Schematic of turbulent jet induced by (a) single-phase and (b) steam to water injection.

2.2. Entrainment Analysis

The volumetric flow rate $\dot{Q}_a$ can be calculated by integrating Eq. (**1**) over *r*.

$$\dot{Q}_a = \int_0^\infty 2\pi r U(x,r)\, dr = \pi d U_0 \frac{B}{K} \cdot (x - x_0) \tag{3}$$

For constant density jets, the relation between the axial $\dot{Q}_a$ and radial $\dot{Q}_r$ volumetric flow rates (Figure 3) can be written as

$$\frac{d\dot{Q}_a(x,R)}{dx} = \dot{Q}_r(x,R) = 2\pi R V_e(x,R) \tag{4}$$

where R is the radius of the control volume, and V_e is the entrainment velocity. By substituting Eqs. (1), (3) and (4)and assuming $\xi = R/(x - x_0)$, we get

$$RV_e(x,R) = \frac{U_0 dB}{2K}\left[1 - (1 + 2K\xi^2)e^{-K\xi^2}\right]. \tag{5}$$

It can be found that the product of the entrainment velocity and the radius $RV_e(x,R)$ is constant along $\xi = R/(x - x_0)$ and for large values of $K\xi^2$ it asymptotically approaches $U_0 dB/2K$.

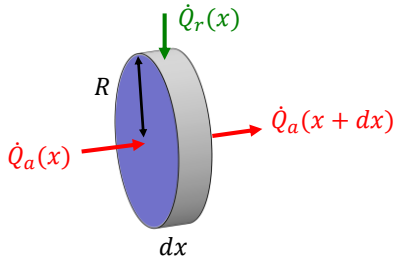

Figure 3 Volumetric flow rate balance in a round jet.

2.3. EHS/EMS Models

Turbulent jet induced by steam condensation is also believed to share similar characteristics at some distance away from the steam condensation region [14]. In other words, the Eqs. (1)~(5) that aimed for the single-phase jet could be referred to describe the condensed jet Figure 2b. Thus, the effective momentum $\dot{M}_{eff}$ rate (EMS) for subsonic steam flow conditions has been proposed and measured, it can be estimated [4] as:

$$\dot{M}_{eff} = C\dot{M}_{th} = C\rho_s A_0 U_s^2 = \rho_l A_0 U_{eff}^2 \tag{6}$$

where C is the condensation regime (or effective momentum) coefficient used to compute how much momentum is created in the process of steam condensation. $\dot{M}_{th}$ is the theoretical momentum rate of injected steam. Subscript s and l represent the steam and liquid; A_0 is the injection hole area; U_{eff} is the effective velocity of the liquid. The effective momentum rate was measured in SEF [4]. The coefficient C can be approximated by an empirical correlation, where ΔT is water subcooling.

$$C = 4.28\Delta T^{-0.35} \tag{7}$$

The effective heat source $\dot{Q}$ is computed by:

$$\dot{Q} = \dot{m}_s h_s \tag{8}$$

where $\dot{m}_s$ and h_s are the mass flow rate and enthalpy of the steam.

3. EXPERIMENTAL SETUP

3.1. SEF-POOL

The overview of SEF-POOL which includes sparger piping and a water pool is presented in Figure 4. The pool is around 1500 mm long, 300 mm depth, and 600 mm tall. The primary goal of the facility is to measure the resultant momentum (collected by PC pipe and disk stack) induced by steam condensation through injection holes. However, the tests discussed in this work were carried out without

the PC pipe and disk stack. Instead, air bubbles were injected through small needles positioned at the bottom of the pool. Eight individual bubble syringes were used in the first few tests and this bubble system was upgraded to a 32-injector system in 2020. Bubble trajectories were recorded by two high-speed cameras with 6300 Frame Per Second (FPS).

More details regarding the facility geometry, cameras, bubble generation system, sparger pipe, illumination, other measurement systems, and performed tests are well introduced in Appendix B of this report [15]. The tests discussed in this paper are summarized in Table 1. The major difference from SEF-W7 to W8 is that the cameras were adjusted to capture more bubbles. Stagnation test where only air bubbles are resealed from the needles (Figure 7) was performed before steam or water injection of each test to measure the rising velocity of bubbles (Figure 10) for the entrainment analysis. The initial water level is $\sim 0.45\ m$ m and pool temperature is ~ 15 ℃.

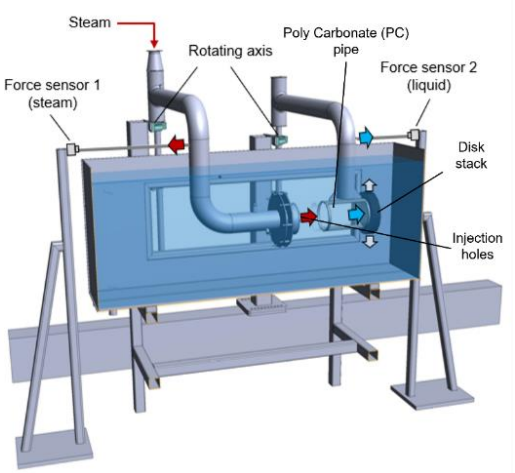

Figure 4 SEF-POOL test facility. PC pipe and disk stack are not involved in the current test.

Table 1. Injection tests in this work

Test	Water/Steam flux $[kg/m^2s]$	Water/effective[1] velocity (m/s)	Hole diameter [mm]	Injected water Temperature [℃]
SEF-W7	-	1.41, 2.59, 3.85	1×16	~12
SEF-W8	-	1.27, 2.95	1×16	~17
SEF-S34	49	~1.85	3×16	~103

[1] Effective velocity estimated by Eqs. (6), (7).

3.2. Image Processing

Main procedures (Figure 5) of image processing to obtain the 3D trajectory of the bubbles are briefly introduced in this section. There are compiled by MATLAB [12]. In the first step, parameters of stereo cameras (two cameras in these tests), including camera intrinsic, distortion, and camera extrinsic, were estimated by the stereo camera calibration by using images that contain a calibration pattern (e.g., checkboard). These parameters could be applied in the later steps to remove lens distortion effects, rectify stereo images, reconstruct a 3D scene, and compute 3D locations corresponding to matched points from two images. By performing the calibration process, the position and orientation of the second camera relative to the first camera can also be obtained. Before each test, a calibration test was performed by putting a checkerboard plate inside the water pool and at least 160 pairs of snapshots could be obtained. This work is summarized in [15].

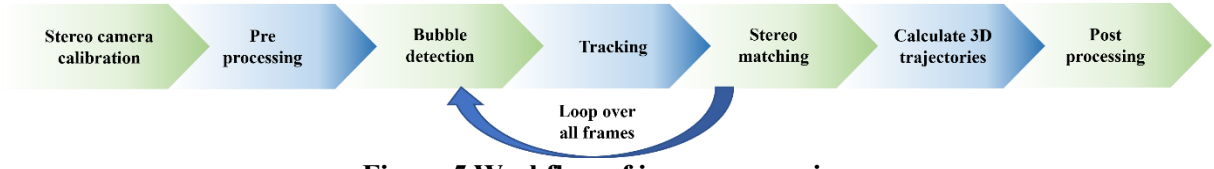

Figure 5 Workflow of image processing

In the second step, bubbles are tracked by several sub-steps. In the first frame, the bubbles are detected separately from two cameras (left and right). The center of mass of the bubbles is recorded and it will be used as the center of the Region of Interest (ROI) window in the next frame to track the bubbles (Figure 6a). The sizes of the ROI window were determined to make sure that the bubble would not escape this region in the next frame.

Calculation of 3D locations of a bubble requires image points of a pair of matched bubbles from two cameras combined with stereo camera parameters from the calibration test. Stereo bubble matching is the most significant part of this work as it determines the correctness of the bubble trajectory and the accuracy of subsequent velocity analysis. Epipolar geometry [19] combined with image registration [18] were used to correlate the bubbles. Generally, as it can be seen from Figure 6b and Figure 7, epipolar geometry provides a solid constraint that the matching point of X_L must fall on the epilolar line in the right view. In other words, the matched points on the images and their corresponding world point must be coplanar and the epipolar line is the projection of this plane on the 2D view.

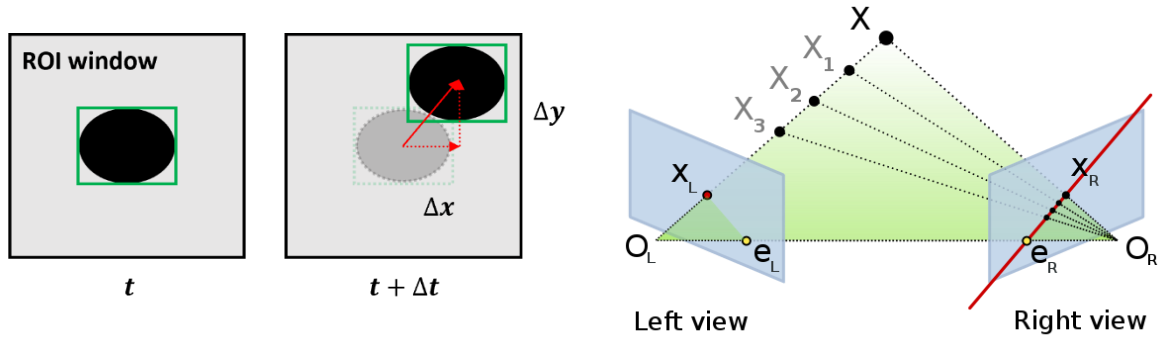

(a) **(b)**

Figure 6 Schematic of (a) bubble tracking using ROI window and (b) epipolar geometry [19].

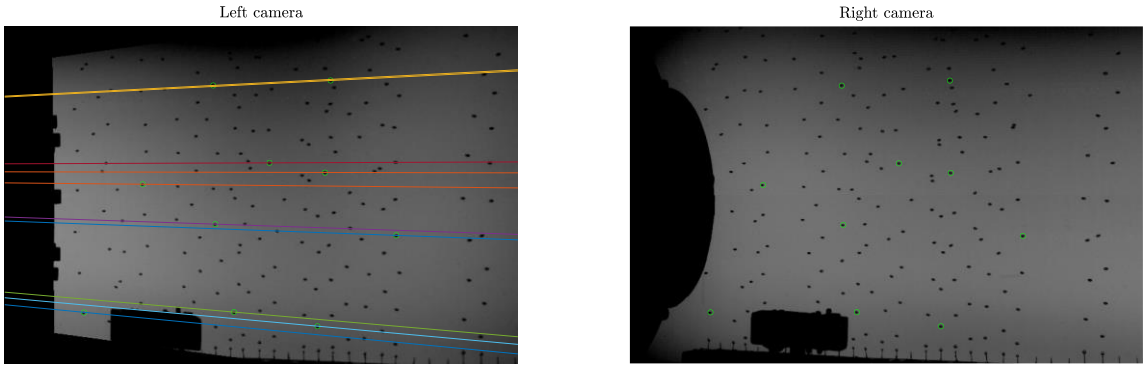

Figure 7 Epipolar lines of multiple bubbles in stagnation test of SEF-W7

As multiple bubbles could fall on the same epipolar line (Figure 7), image registration was applied to narrow down the candidates. For each pixel in one image, image registration tries to find a pixel in another image of the same scene that stereoscopically corresponds to it. After image registration, the matched bubbles are closer to each other as shown in Figure 8. By doing this, the correlation of bubbles can be simply solved by searching for the closest bubble and then checking if it satisfies the epipolar constraint.

Matched bubbles can be found in the stagnation phase (Figure 9) and this is mainly attributed to the fact that the bubbles are not very dense compared to the injection phase (Figure 13b) where bubbles are clustered. Voting mechanism where the bubble is correlated at each frame and then determines the matched bubble by the largest sum of votes could be involved.

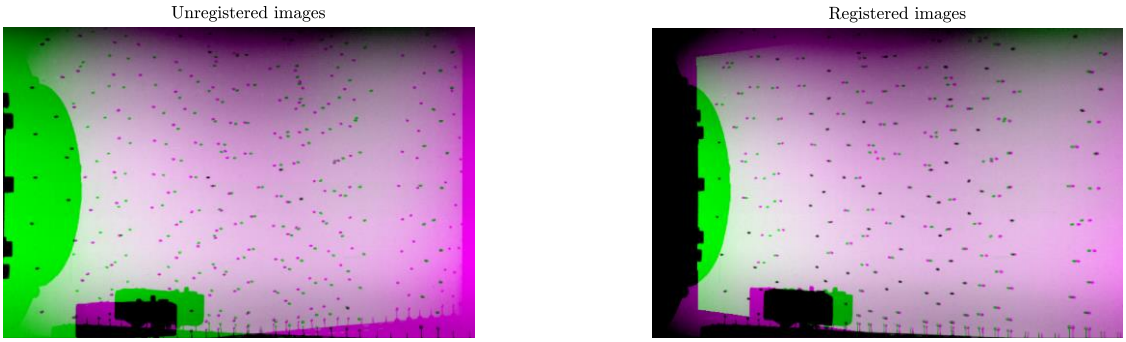

Figure 8 Image registration to close the matched bubbles.

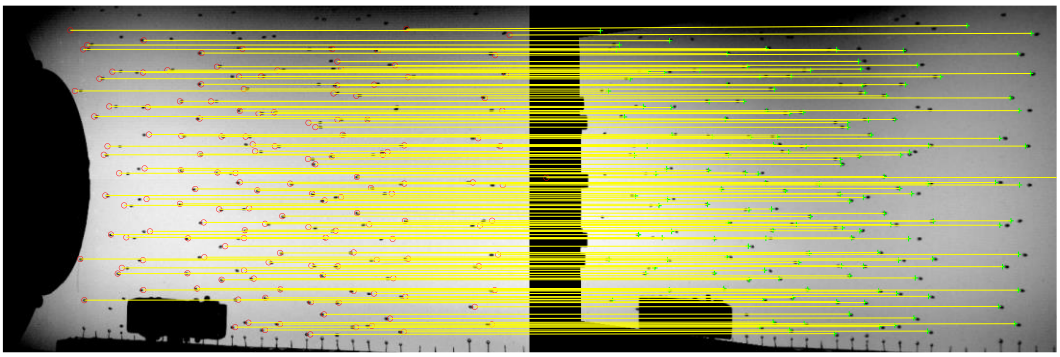

Figure 9 Correlated bubbles in a stagnation test of SEF-W7

3.3. Post Processing of Trajectory

3D trajectories of bubbles are computed by matched bubbles and stereo camera parameters. An example of trajectories obtained in the stagnation test of SEF-W7 is illustrated in Figure 10. The bubbles rise spirally upwards without interacting with ambient bubbles at different trains. Velocity is calculated as:

$$V(t+0.5\Delta t)=\frac{p^{t+\Delta t}(x,y,z)-p^{t}(x,y,z)}{\Delta t} \tag{9}$$

where $p^t(x,y,z)$ is the world coordinate of the bubble at time t, and Δt is the time lag of 0.001587s corresponding to 10 frames with 6300 FPS.

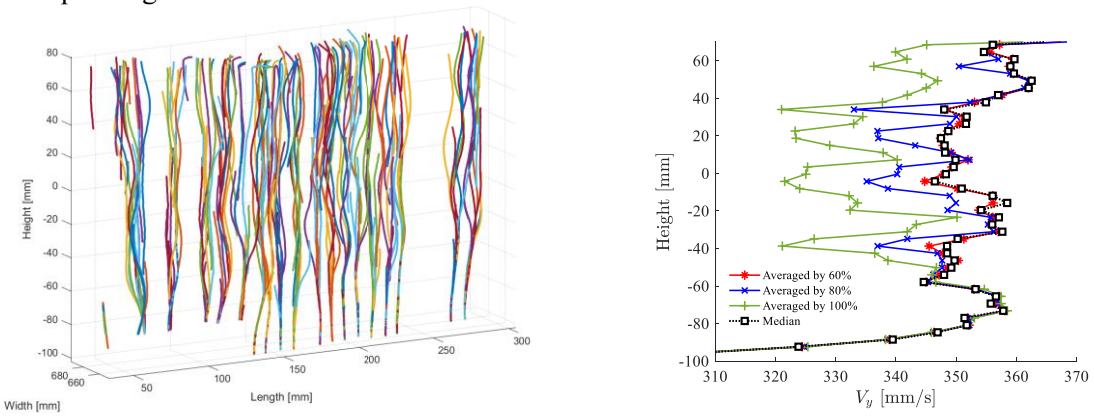

(a) **(b)**

Figure 10 (a) 3D trajectories and (b) rising velocity of bubbles with different averaging methods at L=150 mm in stagnation test of SEF-W7

The flow region was meshed by $16\times32\times1$ (length, height, and depth) blocks in the stagnation phase and $48\times32\times1$ blocks in the injection phase (Figure 11a). Given the flow region was not completely filled by the sparse bubbles, the deep direction was discretized by a single layer to make sure that each

grid contains enough bubbles (Figure 11b) over the whole transients (around 2200 frames). As long as a bubble appears in a grid, it will be counted once. Different averaging strategies for data in a single grid have been investigated and presented in Figure 10b. "Averaged by 60%" indicates that 20% of maximum values and 20% of minimum values are excluded and then averaged by the arithmetic mean. This averaged approach was used in the following tests to calculate the 2D (1 grid in-depth) velocity field over the whole frames (Figure 14).

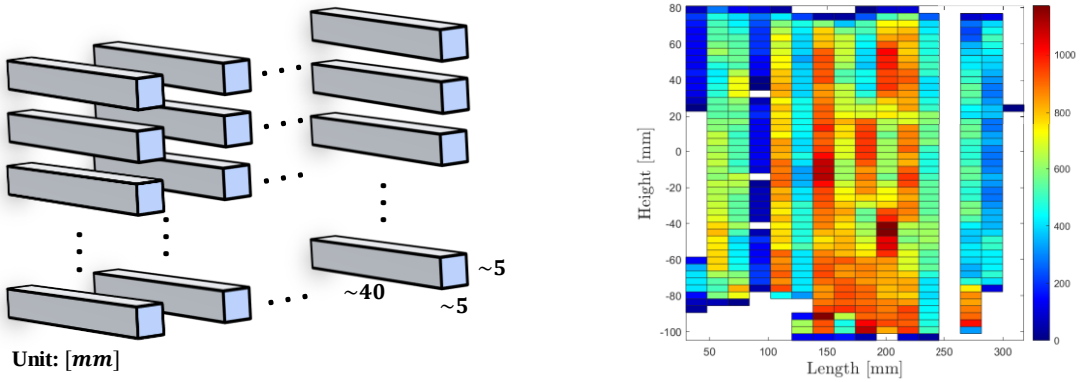

(a) **(b)**

Figure 11 (a) Schematic of mesh used in velocity analysis and (b) number of bubbles in the grid during the whole transient in stagnation test of SEF-W7

4. RESULTS AND DISCUSSION

4.1. CFD Validation

CFD simulations were performed by using ANSYS Fluent 2021 R2 [13]. For the water to water test, single-phase incompressible solver with $k-\epsilon$ realizable model was used. The energy equation was closed. Turbulence is introduced by default turbulent intensity of 5% and turbulent viscosity ratio of 10. Mesh was refined near the injection hole and wall. Steady-state calculations were performed and considered fully converged as all the residual is below 1e-4. These simulations are compared with measurements and analytical results as discussed in the remaining sections. EHS/EMS models were applied to simulate the effective turbulent flow induced by steam condensation. Details can be found in [9, 10].

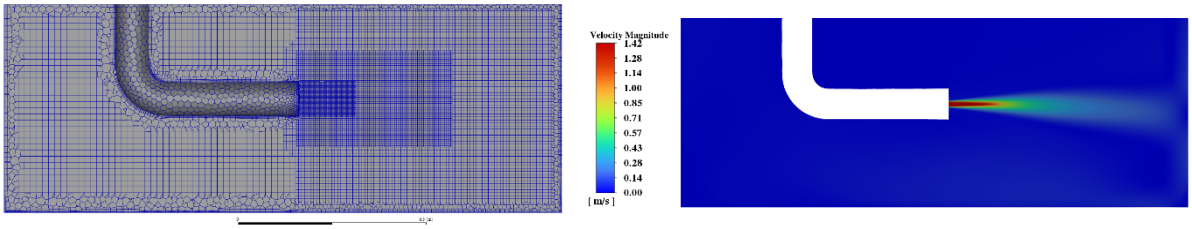

(a) **(b)**

Figure 12 (a) Mid-plane mesh of SEF-POOL and (b) velocity contours with $U_0 = 1.41 m/s$

4.2. Axial Velocity

Axial velocity profiles of the jet induced by water or steam injection can be measured by tracking the bubbles in the main flow. Figure 13 and Figure 16 present the bubble position in the first frame of the SEF-W7 and SEF-S34 tests and its resulting 3D trajectories. A typical movement of the bubble is that it is released from the bottom needle, then rises to the main flow by entrainment and buoyancy, and finally is pushed downstream by the main flow. A small fraction of bubbles can penetrate the main flow and then continue flowing upward.

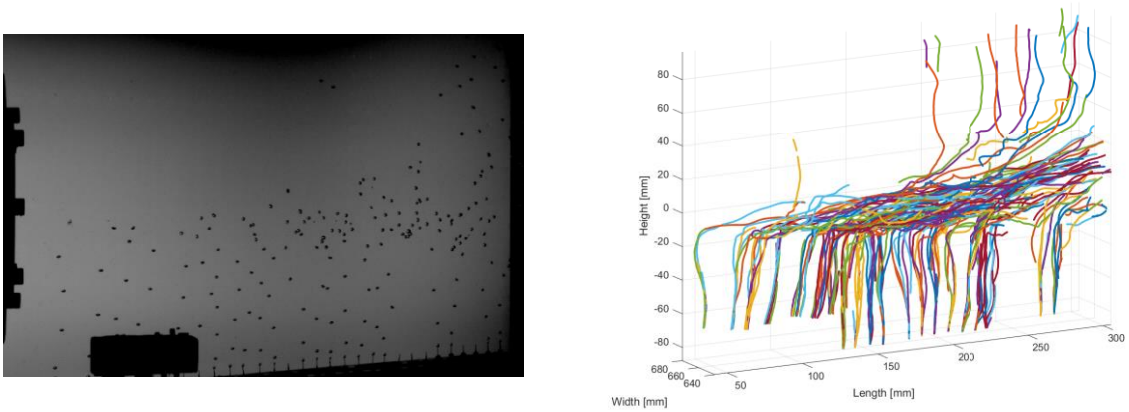

(a) **(b)**

Figure 13 Image of the bubbles in (a) SEF-POOL with water-to-water injection (SEF-W7, $U_0 = 1.41\ m/s$) and (b) resulting 3D trajectories.

Comparison of axial velocity profiles among measurement, CFD simulations, and analytical predictions (single-phase turbulent only) are presented in Figure 14b, Figure 15, and Figure 17b. Analytical solutions were obtained by using Eq. (1) with $K = 50, B = 5, d = 16mm, x_0 = 0.025m$ [16]. Good agreement of centerline velocity between CFD and analytical profile suggests that CFD simulations could provide adequate prediction of the velocity field.

The measurements that are far from the centerline (e.g., $H = -18, -24\ mm$ in SEF-W7) achieve a better agreement compared to the data close to the centerline. Meanwhile, the closer the area to the injection hole, the fewer measurements can be obtained. This is attributed to the lack of bubbles in the core of the flow (Figure 13, Figure 17) where the risen bubbles would be accelerated immediately when they enter the flow. Given the axial velocity of the jet ($1.4\sim3.85\ m/s$) is much greater than the bubble rising velocity ($0.35\ m/s$, Figure 18a), most of the bubbles would escape from the camera view when it rises to the centerline of the jet. The transition of bubbles from vertical rising to horizontal flowing is the major contribution to the oscillated velocity measurement, especially for the near field region where $L \leq 200\ mm$.

In order to take full advantage of the Field of View (FOV) where a longer downstream region can be measured and to exclude the upper part of the region where no or fewer bubbles pass through (Figure 13), the cameras and air bubble generating system are adjusted as shown in Figure 16. The effective downstream region where a reliable measurement can be obtained is extended from around $\sim150-300$ to $\sim150-400\ mm$. This is very helpful for steam-to-water injection tests where condensed steam would impose a negative effect on the region close to the orifice.

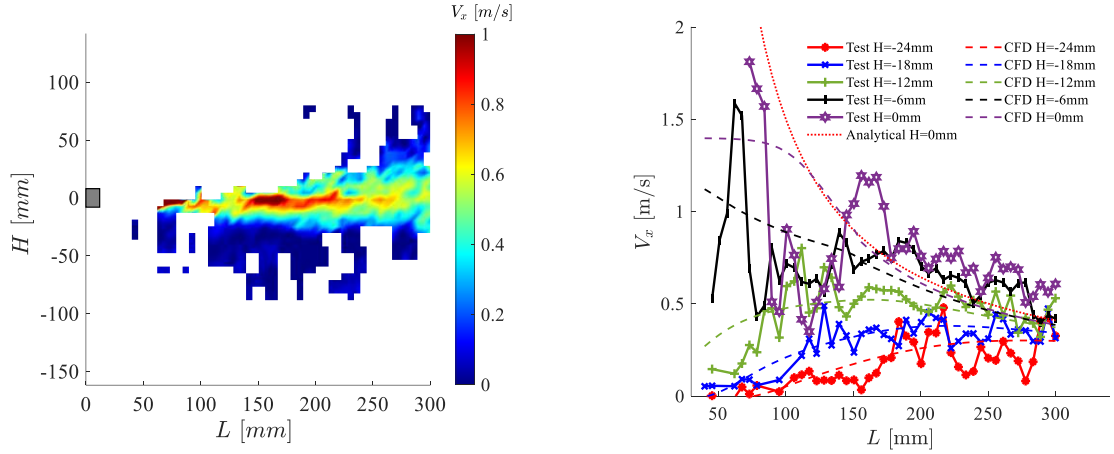

(a) **(b)**

Figure 14 Results of SEF-W7 with $U_0 = 1.41\ m/s$ of (a)velocity contours according to 3D trajectories (b) axial velocity at different height. Data were averaged over 2200 frames.

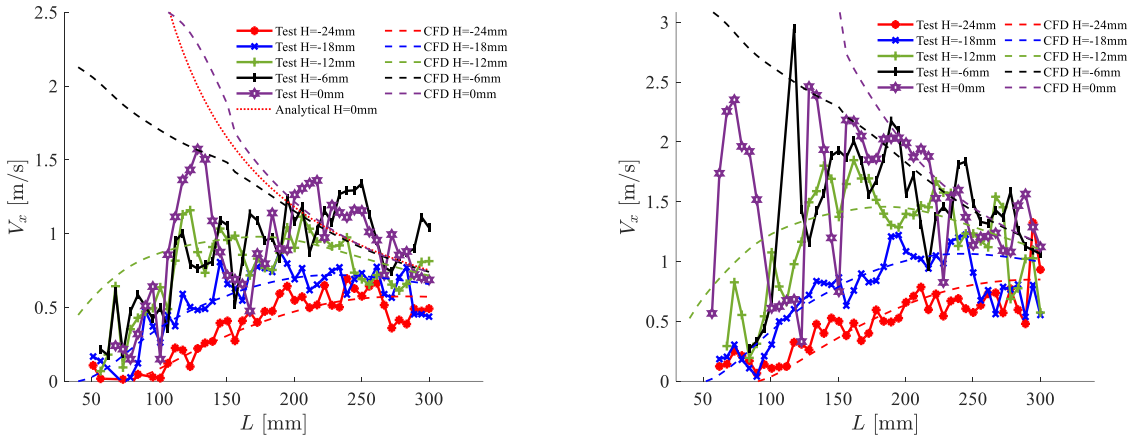

(a) **(b)**

Figure 15 Axial velocity profiles at different heights of SEF-W7 with (a) $U_0 = 2.59\ m/s$ and (b) $U_0 = 3.85\ m/s$. Data were averaged over 2200 frames.

CFD simulation using EHS/EMS models is compared with test measurement as shown in Figure 17b. A relatively larger extra Turbulent Kinetic Energy (TKE) source is required for the condensed steam jet to achieve quite diffused profiles compared to the water jet with a similar amount of momentum (Figure 14b, Figure 15a). This is caused by the oscillation characteristics of the steam jet where intermittently condensed steam behaves like a stick stirring in the water. This high-level turbulence was also observed by the PIV measurement in the large-scale pool tests [5] and by the simulations in [9, 10].

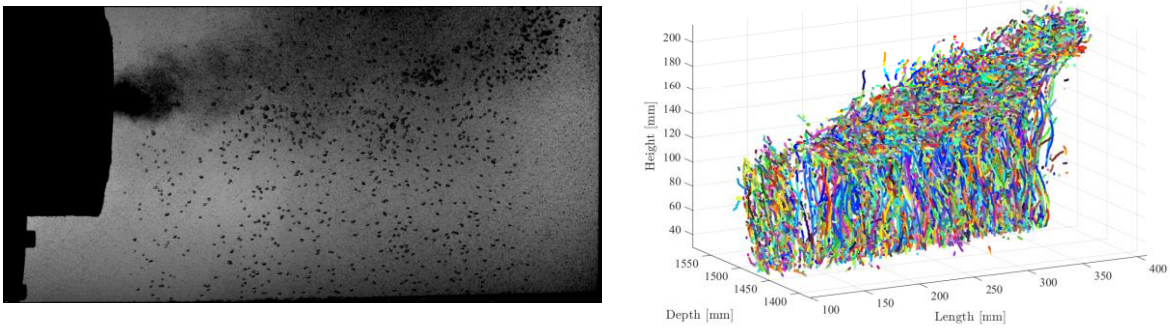

(a) **(b)**

Figure 16 Image of the bubbles in (a) SEF-POOL with steam-to-water injection (SEF-S34) and (b) resulting 3D trajectories.

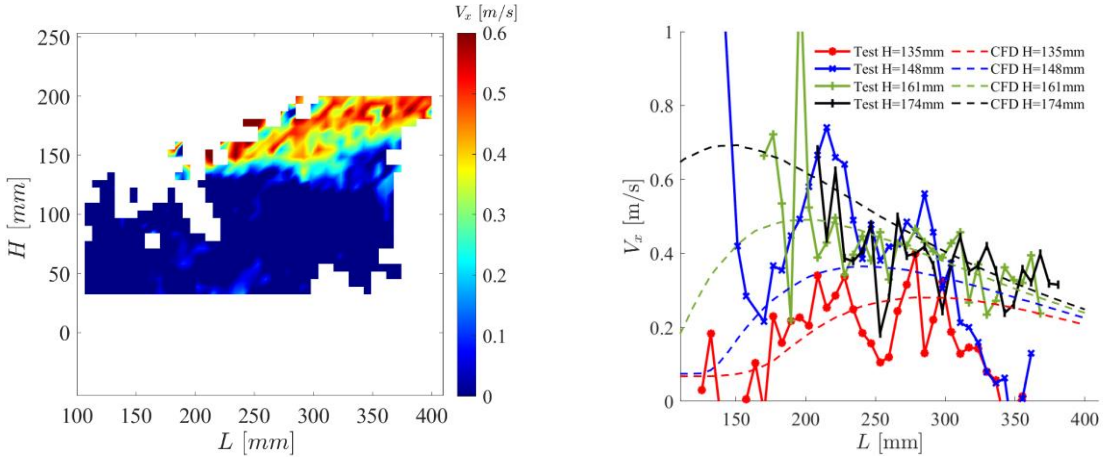

(a) **(b)**

Figure 17 Image of the bubbles in (a) SEF-POOL with steam-to-water injection (SEF-S34) and (b) resulting 3D trajectories.

4.3. Entrainment Analysis

The product of the entrainment velocity and radial distance (V_yR) in SEF-W8 with $U_0 = 2.95\,m/s$ is compared with CFD simulations and analytical solutions (Figure 18b). The entrainment velocity was calculated by taking the difference between the measured rising velocity in injection phase and the reference rising velocity in the stagnation phase. The deviation of V_yR between CFD simulations and analytical solutions estimated by Eq. (5) is expected since the Eq. (5) is developed based on the infinite boundary while the facility is a restricted pool.

The original idea of this series of experiments is to deduce the diffusion of the turbulent jet by measuring the entrainment of the bubbles (see Eqs. (3)~(5)). However, later post-processing [12] suggests that the uncertainty of the bubble rising velocity (~$50\,mm/s$, Figure 10b, Figure 18a) is larger than or has the same order as the velocity induced by main flow entrainment (~$50\,mm/s$, with $U_0 = 2.95\,m/s$ at $R = 50\,mm$, as shown in Figure 18b), making it is impossible to accurately measure the net entrainment velocity and subsequently determine the main flow characteristics. As the ultimate goal is to deduce the momentum distribution downstream of the steam condensation induced jet, direct measurement of axial flow velocity should be the priority if there are enough bubbles that could be tracked in the main flow. While, for those cases with high axial velocity, entrainment measurement could be considered as a backup solution.

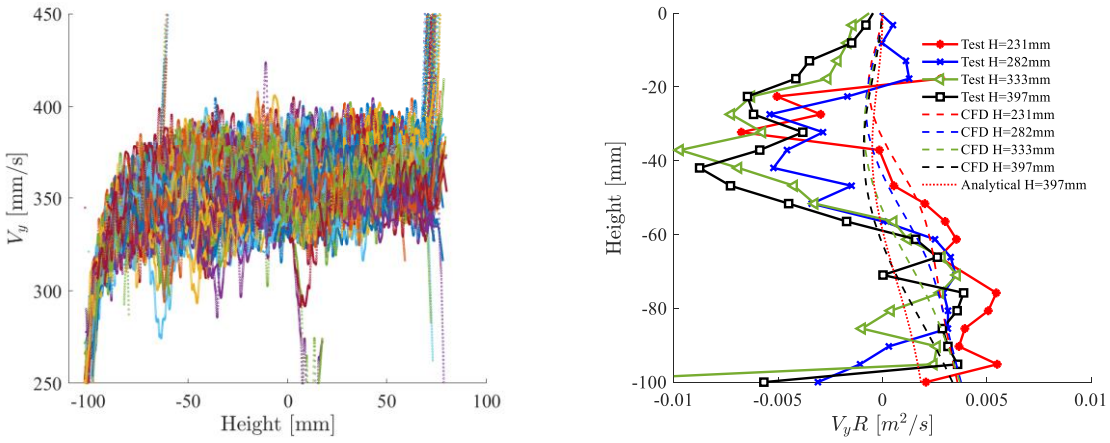

(a) **(b)**

Figure 18 (a) rising velocity profiles of all bubbles in stagnation test and (b) the product of entrainment velocity and radial distance in SEF-W8 with $U_0 = 2.95\,m/s$

5. CONCLUSIONS

In this work, we have demonstrated the ongoing process of designing an experimental method for the measurement of velocity induced by water/steam injection. Measurement of the bubbles away from the centerline provides a better agreement compared to the bubbles in the main flow. Turbulent flow induced by steam injection diffuses much faster than the single-phase turbulent flow with the same amount of momentum, indicating an extra turbulent kinetic energy source is necessary for setting the boundary conditions of EHS/EMS models. Stereo cameras should be adjusted as SEF-S34 where bubbles could fill up the field of view. Direct measurement of axial velocity by tracking the downstream bubbles provides less uncertainty than the measurement of entrained bubbles when the injection velocity is small.

ACKNOWLEDGMENTS

The authors would like to thank the experimental team at Lappeenranta University of Technology (Finland) for carrying out SEF experiments.

REFERENCES

1. Pershagen, B., "Light Water Reactor Safety," Chapter 8, Pergamon Press (1994).
2. Li, H., Villanueva, W., Kudinov, P., "Approach and Development of Effective Models for Simulation of Thermal Stratification and Mixing Induced by Steam Injection into a Large Pool of Water". *Science and Technology of Nuclear Installations*, Article ID 108782, (2014).
3. Gallego-Marcos, I., Kudinov, P., Villanueva, et al., "Pool Stratification and Mixing Induced by Steam Injection through Spargers: CFD modeling of the PPOOLEX and PANDA experiments", *Nucl. Eng. Des*, 347, 67-85 (2019).
4. Gallego-Marcos, I., Kudinov, P., Villanueva, et al, "Effective momentum induced by steam condensation in the oscillatory bubble regime", *Nucl. Eng. Des*, 350, 259-274 (2019).
5. Gallego-Marcos, I., Kudinov, P., Villanueva, et al., "Pool Stratification and Mixing Induced by Steam Injection through Spargers: analysis of the PPOOLEX and PANDA experiments". *Nucl. Eng. Des*, 337, 300-316 (2018).
6. Kapulla, R., Mignot, G., et al., "PIV Measurements in the Vicinity of a Steam Sparger in the PANDA Facility". *Nucl. Eng. Des*, 336, 112-121 (2018).
7. Wang, X., Grishchenko, D., Kudinov, P. "Pre-Test Analysis for Study of Velocity Field of Turbulent Jet Induced by Steam Injection through Multi-hole sparger," *ICAPP-2021*, Abu Dhabi, UAE, October 16-20 (2021).
8. Wang, X., Grishchenko, D., Kudinov, P. "Pre-test analysis for definition of steam injection tests through multi-hole sparger in PANDA facility", *Nucl. Eng. Des*, *386*, 111573 (2021).
9. Wang, X., Grishchenko, D., Kudinov, P. "Modeling of large pool response to steam injection through spargers using A "UnitCell" model", NURETH-19, Brussel Belgium, March 6–11 (2022).
10. Wang, X., Grishchenko, D, Kudinov, P. "Development of Effective Momentum Model for Steam Injection Through Multi-Hole Spargers: Unit Cell Model". ICONE-28. Virtual, Online. August 4–6 (2021).
11. Wang, X., Gallego-Marcos, I., Grishchenko, D., Kudinov, P. "Post-test calibration of the Effective Momentum Source (EMS) model for steam injection through multi-hole spargers", NURETH-18. Portland, USA, 6176-6189, August 18–23 (2019).
12. MATLAB®, version 2021b. Natick, Massachusetts: The MathWorks Inc.
13. ANSYS® Fluent Theory Guide, Release 2021 R2.
14. Chul-Hwa Song, Seok Cho, Hyung-Seok Kang. "Steam Jet Condensation in a Pool: From Fundamental Understanding to Engineering Scale Analysis." *ASME. J. Heat Transfer* Vol. 134(3), 031004 (2012).
15. Kudinov, P., Wang, X., Grishchenko, D., et al., "Thermal Hydraulic Phenomena of the Suppression Pool - Summary of 2020 activities". NKS-THEOS Report. NKS-450 (2021).
16. Pope, S. B., *Turbulent Flows*, Cambridge University Press, Cambridge (2000).
17. Cha. J.H, et al "The effect of the Reynolds number on the velocity and temperature distributions of a turbulent condensing jet", International Journal of Heat and Mass Transfer, 67, 125-132 (2017).
18. Hartley, R., A. Zisserman, *Multiple View Geometry in Computer Vision*, Cambridge University Press, Cambridge (2003).
19. "Epipolar Geometry," https://en.wikipedia.org/wiki/Epipolar_geometry.
20. Grishchenko, D., Wang, X., Kudinov, P. "Towards Assessment of Entrainment of a Water Jet Induced by Steam Injection into a Subcooled Pool", NURETH-19, Brussel Belgium, March 6–11 (2022).